

Mosaic structure ZnO formed by secondary crystallization with enhanced photocatalytic performance

Hai-xia Liu, Meng-yuan Teng, Xu-guang Wei, Tian-duo Li, Zai-yong Jiang, Qing-fen Niu, and Xu-ping Wang

Cite this article as:

Hai-xia Liu, Meng-yuan Teng, Xu-guang Wei, Tian-duo Li, Zai-yong Jiang, Qing-fen Niu, and Xu-ping Wang, Mosaic structure ZnO formed by secondary crystallization with enhanced photocatalytic performance, *Int. J. Miner. Metall. Mater.*, 28(2021), No. 3, pp. 495-502. <https://doi.org/10.1007/s12613-020-2033-0>

View the article online at [SpringerLink](#) or [IJMMM Webpage](#).

Articles you may be interested in

Hong-pan Liu, Xiao-feng Huang, Li-ping Ma, Dan-li Chen, Zhi-biao Shang, and Ming Jiang, [Effect of Fe₂O₃ on the crystallization behavior of glass-ceramics produced from naturally cooled yellow phosphorus furnace slag](#), *Int. J. Miner. Metall. Mater.*, 24(2017), No. 3, pp. 316-323. <https://doi.org/10.1007/s12613-017-1410-9>

Zhen Wang, Hao-yan Sun, and Qing-shan Zhu, [Effects of the continuous cooling process conditions on the crystallization and liberation characteristics of anosovite in Ti-bearing titanomagnetite smelting slag](#), *Int. J. Miner. Metall. Mater.*, 26(2019), No. 9, pp. 1120-1128. <https://doi.org/10.1007/s12613-019-1830-9>

Ze-yun Cai, Bo Song, Long-fei Li, Zhen Liu, and Xiao-kang Cui, [Effect of CeO₂ on heat transfer and crystallization behavior of rare earth alloy steel mold fluxes](#), *Int. J. Miner. Metall. Mater.*, 26(2019), No. 5, pp. 565-572. <https://doi.org/10.1007/s12613-019-1765-1>

Huan-huan Wang, Wen-xiu Liu, Jing Ma, Qian Liang, Wen Qin, Patrick Osei Lartey, and Xiao-jiang Feng, [Design of \(GO/TiO₂\)_N one-dimensional photonic crystal photocatalysts with improved photocatalytic activity for tetracycline degradation](#), *Int. J. Miner. Metall. Mater.*, 27(2020), No. 6, pp. 830-839. <https://doi.org/10.1007/s12613-019-1923-5>

Hui-bin Yang, Feng-qin Liu, and Xiao-lin Pan, [Mineral structure and crystal morphologies of high-iron hydrargillite](#), *Int. J. Miner. Metall. Mater.*, 25(2018), No. 5, pp. 505-514. <https://doi.org/10.1007/s12613-018-1597-4>

Yong Zhang, Zhao-hui Guo, Zi-yu Han, Xi-yuan Xiao, and Chi Peng, [Feasibility of aluminum recovery and MgAl₂O₄ spinel synthesis from secondary aluminum dross](#), *Int. J. Miner. Metall. Mater.*, 26(2019), No. 3, pp. 309-318. <https://doi.org/10.1007/s12613-019-1739-3>



IJMMM WeChat



QQ author group

Mosaic structure ZnO formed by secondary crystallization with enhanced photocatalytic performance

Hai-xia Liu¹, Meng-yuan Teng¹, Xu-guang Wei¹, Tian-duo Li¹, Zai-yong Jiang², Qing-fen Niu¹,
and Xu-ping Wang³

1) Shandong Provincial Key Laboratory of Molecular Engineering, School of Chemistry and Pharmaceutical Engineering, Qilu University of Technology (Shandong Academy of Sciences), Jinan 250353, China

2) State Key Laboratory of Biobased Material and Green Papermaking, Qilu University of Technology (Shandong Academy of Sciences), Jinan 250353, China

3) Advanced Materials Institute, Qilu University of Technology (Shandong Academy of Sciences), Jinan 250014, China

(Received: 24 December 2019; revised: 2 March 2020; accepted: 4 March 2020)

Abstract: Zinc acetate is used as a raw material to synthesize the desired ZnO in hot solvent by controlling the amount of citric acid (CA) added. Notably, the amount of CA added has a significant relationship with the control of the morphology of ZnO. Spherical ZnO wrapped in nanosheets is synthesized through the secondary crystallization of Zn²⁺. The optical properties of the ZnO sample are tested through the degradation of organic pollutants. Notably, the photocatalytic properties of ZnO vary with the different amounts of CA added. Exposure of the active crystal face increases the photocatalytic activity of ZnO. In addition, the number of defects on the surface of the ZnO sample increases because of its large specific surface area, thus changing the bandgap of ZnO. Therefore, the resulting sample can respond under visible light.

Keywords: active crystal face; citric acid; secondary crystallization; photocatalysis

1. Introduction

In recent years, with the continuous development of the social economy, the environmental problems on Earth have become increasingly serious, particularly the pollution of water resources [1]. Severe shortage of water resources is occurring in most parts of the world because of climate change and poor water resource management. Thus, water resource recycling, purification, and reuse technologies have attracted considerable attention. As a kind of photocatalyst [2–3], semiconductor materials can effectively degrade wastewater by completely transforming organic pollutants into H₂O and CO₂ [4–6]. Compared with many other semiconductor materials, ZnO has the advantages of nontoxicity, high electron mobility, high efficiency, and low cost [7–9]. However, ZnO, as a photocatalyst, also has some inherent limitations, such as rapid recombination of photogenerated carriers, wide bandgap (3.37 eV), low solar energy utilization, and vulnerability to photo etching [10–11]. To improve the photocatalytic performance of ZnO, scientists have conducted a number of material development studies, such as coupling with noble metal ions [12–13], combining with semiconductor

materials [14–15], and doping with nonmetals [16–17].

Evidently, exposing the active crystal faces of ZnO is also a good method to improve its photocatalytic performance. Photocatalytic performance is closely related to the electronic structure of the surface of the photocatalyst because photocatalytic reactions occur on the surface of the photocatalyst and other reactants [18–19]. According to scientists, exposure of the active crystal faces of ZnO has important effects on its photocatalytic properties [20–21]. Scientists have also proven that the (0001) crystal plane of ZnO is an important active crystal plane and has a significant relationship with its photocatalytic properties [22]. Exposure of the (0001) crystal plane of ZnO to different reaction conditions has become the main direction of research. Therefore, selecting the growth direction of ZnO to expose more of its (0001) crystal planes is one of the keys to increase its catalytic activity [23]. At the same time, scientists have introduced the concept of interface defects to improve the solar energy utilization of pure ZnO. The formation of defects at the conduction band (CB) of ZnO without introducing other elements provides an effective method for visible light catalysis [7,24]. The most important influencing factor is the oxygen vacancy defect on the

surface of ZnO. Notably, the oxygen vacancy defect on the surface of ZnO can narrow the bandgap of ZnO and make it respond under visible light [24]. The visible light catalytic process is largely dependent on the surface properties of ZnO [25–26]. In the photocatalytic process, the surface defects of ZnO can capture and transfer electrons to the surface of the semiconductor, thereby improving the separation efficiency of photogenerated electrons and holes [27]. A previous investigation determined that the photocatalytic performance of pure ZnO depends mainly on the type and density of surface defects [28]. Therefore, the construction of a large specific surface area of ZnO photocatalyst increases the concentration of surface defects, thus improving the visible light catalytic activity [29].

In this study, ZnO is synthesized through a simple solvothermal method. The solvothermal method can easily control the morphology of ZnO. The morphology of the special mosaic structure ZnO is controlled by changing the amount of citric acid (CA) added. The effect of different amounts of CA on the special morphology of ZnO is examined. In addition, exposure of the active crystal face of ZnO can increase its photocatalytic activity. The (0001) active crystal faces of ZnO can be exposed by changing the amount of CA added. Similarly, the surface oxygen vacancies of ZnO can narrow the bandgap of ZnO. Moreover, a large specific surface area can increase the concentration of surface defects, thereby increasing the visible light catalytic performance of pure ZnO. A battery of characterization methods are used to investigate the morphology of ZnO. The photocatalytic properties of the ZnO sample are also tested through the degradation of rhodamine B (RhB).

2. Experimental

2.1. Materials

Zinc acetate ($(\text{CH}_3\text{COO})_2\text{Zn}\cdot 2\text{H}_2\text{O}$) and citric acid monohydrate ($\text{C}_6\text{H}_8\text{O}_7$) were purchased from Sinopharm Chemical Reagent Co. Ltd., China. Absolute ethanol ($\text{C}_2\text{H}_5\text{OH}$) was purchased from Tianjin Fuyu Chemical Co. Ltd., China. All chemicals used in this work were of analytical grade and used as received without further purification. Distilled water was used throughout the experiment.

2.2. Synthesis of ZnO spheres

First, 0.329 g $(\text{CH}_3\text{COO})_2\text{Zn}\cdot 2\text{H}_2\text{O}$ was added to 30 mL absolute ethanol solution and stirred until completely dissolved. Then, 0.025 g $\text{C}_6\text{H}_8\text{O}_7$ was weighed, added to the solution, and stirred continuously. The mixed solution was stirred for 30 min and then transferred to a Teflon-lined reaction vessel. The reaction vessel was closed and kept for 4 h at 160°C. After cooling to normal temperature, the sample was suction filtered, washed, and dried to obtain the desired product. Under the same conditions, the amount of CA ad-

ded was adjusted to obtain different products.

2.3. Measurement of photocatalytic performance

The photocatalytic performance of ZnO was measured through the decomposition of RhB, which was used as the target pollutant. First, 0.1 g of the sample was dispersed in 100 mL RhB solution at room temperature. Then, the mixed solution was stirred continuously in the dark (1 h) to achieve adsorption equilibrium on the surface of the catalyst. Subsequently, a certain amount of the solution was aspirated into the test tube every 10 min. Finally, a given mass of supernatant was measured using a UV–Vis spectrophotometer.

2.4. Characterization instruments

X-ray diffractometer (Bruker D8, Cu K_α radiation, $\lambda = 0.1540562$ nm), environmental scanning electron microscope (SEM, Hitachi S-4800), field emission high-resolution transmission electron microscope (HRTEM, JEM-2100F), UV–Vis spectrophotometer (DRS, Shimadzu UV-3600), and specific surface area aperture analyzer (GeminiV2380) were the instruments used in this study.

3. Results and discussion

ZnO synthesized with different amounts of CA added was measured through X-ray diffraction (XRD). From Fig. 1, the distinguishable peaks at 31.7°, 34.4°, 36.3°, 47.6°, 56.5°, 62.9°, and 67.9° corresponded to the (100), (002), (101), (102), (110), (103), and (112) planes of hexagonal wurtzite ZnO (JCPDS No. 36-1451). In addition, no other diffraction peaks were detected in the XRD patterns. The narrow-tip peaks confirmed that the samples exhibited good crystallinity. When a large amount of CA was added, the crystallization of ZnO would be reduced; thus, the peak strength would be reduced.

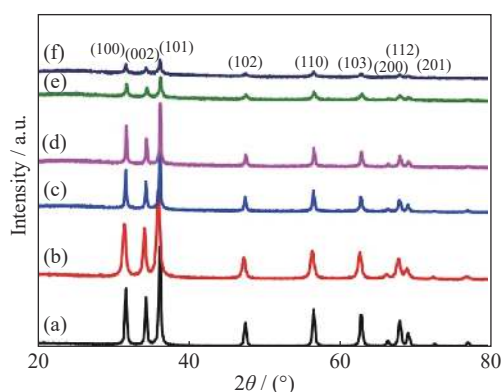


Fig. 1. XRD patterns of ZnO synthesized with different amounts of CA added: (a) 0.000 g CA; (b) 0.010 g CA; (c) 0.025 g CA; (d) 0.050 g CA; (e) 0.075 g CA; (f) 0.100 g CA.

The morphology of the synthesized ZnO was investigated by SEM characterization. Fig. 2 shows the SEM images of

ZnO when the amount of CA added is 0.025 g. As shown in Fig. 2, when CA was used as an additive, the morphology of the resulting product was a ZnO micro/nanosphere. ZnO micro/nanospheres had a diameter of approximately 2 μm. The surface of the sphere had a number of nanosheets embedded in it, which formed its special structure. The thickness of the nanosheets was approximately several tens of nanometers. Figs. 2(c) and 2(d) show that the nanosheets were uniformly dispersed on the surface of the ZnO sphere, thus increasing

the specific surface area of ZnO. In addition, the active crystal face of each nanosheet was exposed on the surface of the sphere, which enhanced the photocatalytic activity of ZnO [30].

ZnO micro/nanospheres with different morphologies were obtained when different amounts of CA were added. As shown in Figs. 3(a) and 3(b), when the amount of CA added was 0.010 g, the ZnO micro/nanopellets were clustered together. The diameter of the ZnO spheres was approximately

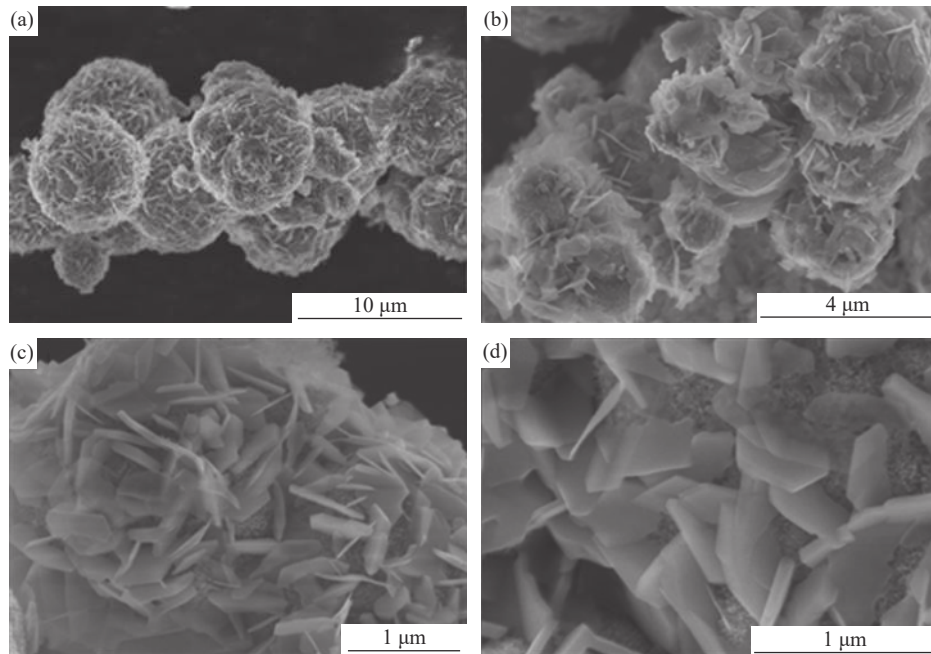


Fig. 2. SEM images of a ZnO sample synthesized by the addition of 0.025 g CA.

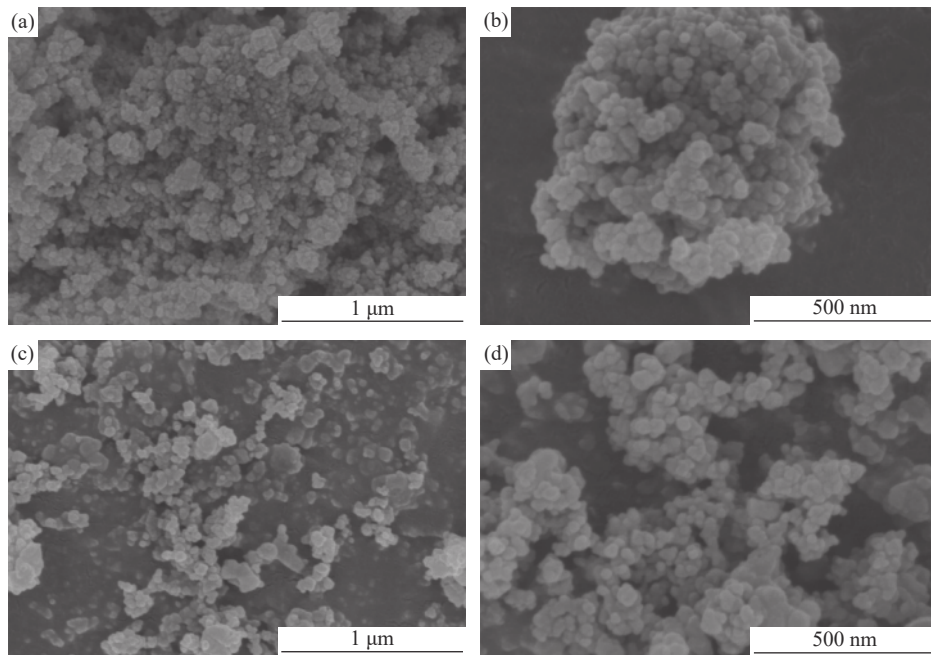


Fig. 3. SEM images of ZnO samples with (a, b) 0.010 g CA and (c, d) 0.050 g CA added.

50 nm. In addition, the surface of the sphere was smooth, indicating that ZnO nanosheet was not formed. This finding can be attributed to the small amount of CA added. Because of its dense distribution, ZnO nanospheres had a relatively small specific surface area. When the amount of CA added was 0.050 g, the shape of the ZnO sphere changed. The morphology of ZnO became an irregular aggregate morphology. The surface of ZnO was covered with nanosheets, and ZnO spheres with irregular aggregate morphology were clustered together. Therefore, secondary crystalline nanospheres could not be formed because of excessive or inadequate amount of additive. The addition of CA had a significant influence on the structure and morphology of ZnO.

HRTEM was further used to verify the structure of ZnO when the amount of CA added was 0.025 g. As shown in Fig. 4(a), ZnO had a special spherical shape, consistent with those

displayed in the SEM images (Fig. 2). The flakes scattered around the ZnO microspheres were flaky ZnO detached from the ZnO microspheres during the grinding process. The selected area electron diffraction (SAED) image (inset in Fig. 4(a)) showed a polycrystalline structure. The reason for this finding was that the selected area exhibited a plurality of single crystals overlapping each other. Figs. 4(b) and 4(c) illustrate the partially enlarged views of the periphery of ZnO micro/nanosphere and the lattice fringe, respectively. Fig. 4(c) shows a plurality of consecutive lattice fringes representing the (10 $\bar{1}$ 0) crystal planes of ZnO. Therefore, the (0001) active crystal planes perpendicular to these consecutive lattice fringes were exposed. The results of HRTEM and SAED indicated that preferential growth units of the sample existed along other axis directions, which resulted in the formation of ZnO with the exposure of the (0001) surface.

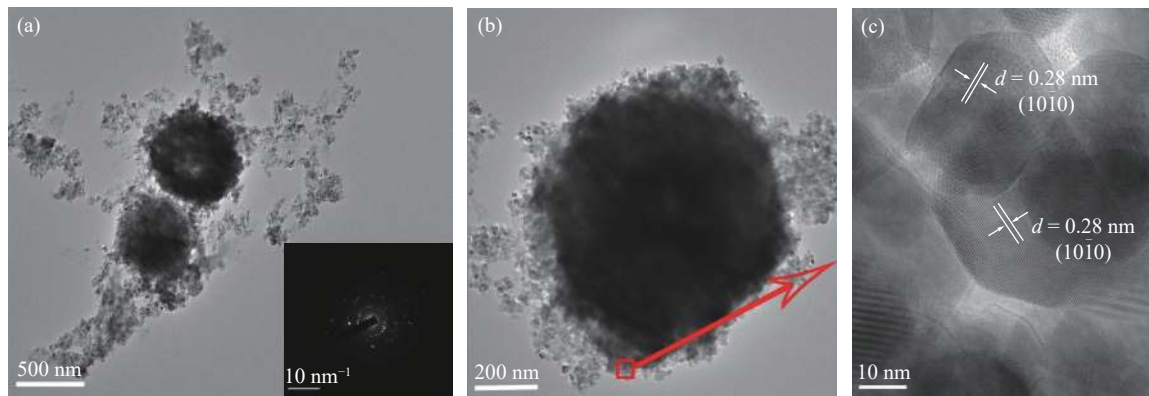


Fig. 4. (a, b) TEM and (c) HRTEM images of ZnO with the addition of 0.025 g CA. Inset in (a) shows the SAED image of 0.025 g CA.

On the basis of the observation and analysis of the SEM and HRTEM images, the growth mechanism of ZnO nanostructures is shown in Fig. 5. First, on the basis of the chemical reaction kinetics, under the appropriate conditions and with the greater degree of supersaturation, the nucleation rate of the grains is significantly higher than its growth rate. Therefore, ZnO micro/nanospheres are rapidly formed

[31–32]. The diffused Zn^{2+} ion forms a chelate with the citrate ion in the solution [33]. The two main forms of Zn^{2+} in solution are growth unit $(Zn(OH)_4^{2-})$ and chelate $(Zn(CA)_2^{10-})$. The chelate is deposited on the (0001) crystal plane of ZnO. Because of the electrostatic repulsion of the same charge, the crystal growth unit is deposited on the other crystal surfaces. Consequently, the growth rate of the (0001)



Fig. 5. Diagram of the growth mechanism of ZnO nanostructures.

crystal plane of ZnO is lower than those of other crystal planes. The resulting sheet-like ZnO is embedded in the surface of the initially formed ZnO sphere [34]. Because of secondary crystallization, the active crystal surface of ZnO is exposed, which improves the photocatalytic activity of ZnO.

The X-ray photoelectron spectroscopy (XPS) spectra of ZnO with the addition of 0.025 g CA were recorded, as

shown in Fig. 6. The sample clearly consisted of Zn and O. As shown in Fig. 6(a), the peaks at 1020.68 and 1043.82 eV correspond to the Zn 2p_{3/2} and Zn 2p_{1/2} peaks, respectively. As shown in Fig. 6(b), the peak at 528.79 eV corresponds to the Zn–O bond, and the peak at 531.32 eV is attributed to the H–O bond in the H₂O molecule on the surface of the sample.

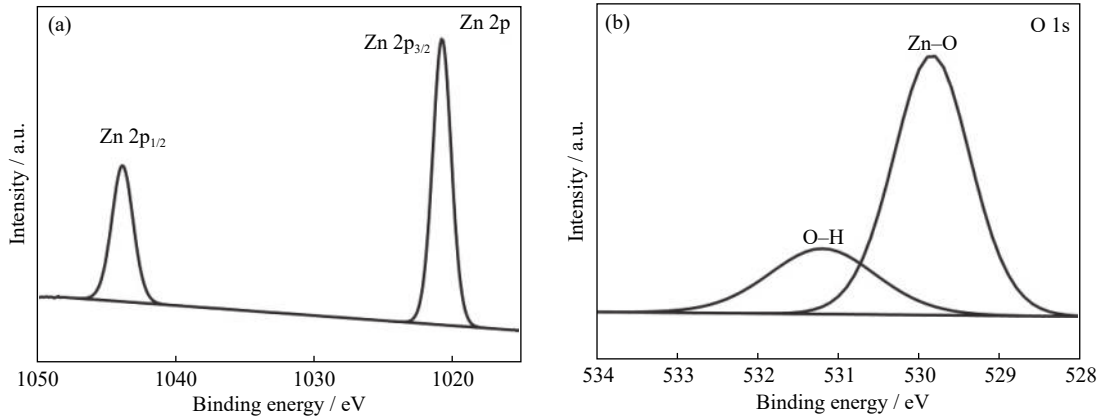


Fig. 6. High-resolution XPS spectra of ZnO with the addition of 0.025 g CA: (a) Zn; (b) O.

The specific surface area of ZnO synthesized with different amounts of CA added was measured using the N₂ adsorption–desorption isotherms obtained by the Brunauer–Emmett–Teller (BET) method (Fig. 7(a)). The isotherms of the samples exhibited typical type IV curves, which represented the characteristics of the mesoporous structure. The BET surface areas of ZnO synthesized with different amounts of CA added were 19.94, 21.03, 60.88, 53.28, 43.63, and 43.39 m²·g⁻¹, as shown in Table 1. Notably, the specific surface area of the synthesized ZnO was the largest when the amount of CA added was 0.025 g. Without the addition of CA, the ZnO sample was formed by dense spherical particles. When CA is added, a mosaic structure ZnO with a secondary crys-

tal structure is formed, which increases the number of holes, thereby increasing the specific surface area. Thus, the specific surface area of ZnO was increased by controlling the amount of CA added, which in turn increased the number of photocatalytic active sites and enhanced the photocatalytic activity. Similarly, a large specific surface area could improve the density of defects on the surface of ZnO, thereby improving the visible light catalytic activity of ZnO [29]. The pore size distribution chart (inset in Fig. 7(a)) shows that the pore size range of ZnO was 2–55 nm. When the amount of CA added was 0.025 g, the pore volume of the sample was the largest.

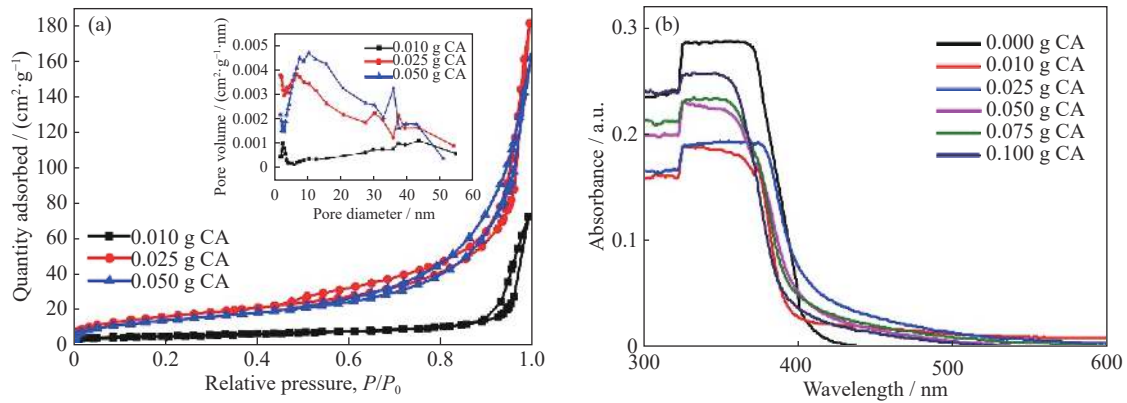
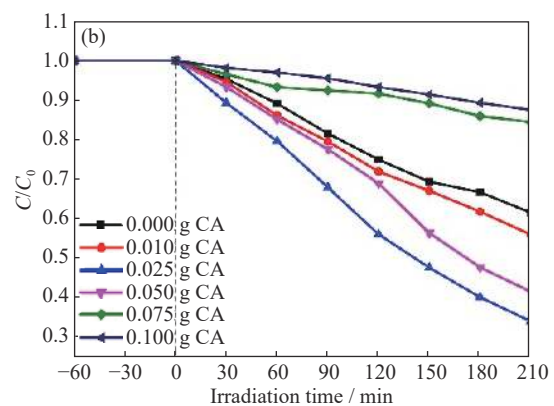
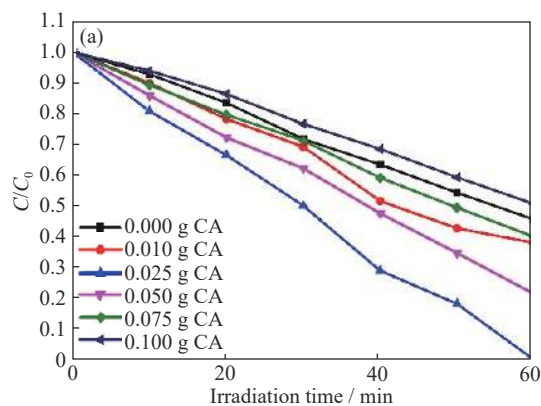


Fig. 7. (a) N₂ adsorption–desorption isotherms and (b) UV–Vis diffuse reflectance spectra of the ZnO synthesized with different amounts of CA added. Inset in (a) corresponds the pore size distribution curves of the ZnO samples (*P*—Pressure of the gas in equilibrium at adsorption temperature; *P*₀—Saturated vapor pressure of gas at adsorption temperature).

Table 1. BET surface areas of ZnO synthesized with different amounts of CA added

Amount of CA / g	BET surface area / (m ² ·g ⁻¹)
0.000	19.94
0.010	21.03
0.025	60.88
0.050	53.28
0.075	43.63
0.100	43.39

The optical properties of ZnO synthesized with different amounts of CA added were observed from the UV–Vis diffuse reflectance spectra. The absorption of ZnO was high in the UV range because of electronic transitions (Fig. 7(b)). As shown in the figure, the critical peak of ZnO appeared at approximately 400 nm. The position of the critical peak of ZnO was shifted to different extents because of the difference in the amount of CA added. The reason for this finding was that the oxygen vacancy defect on the surface of ZnO can narrow the bandgap of ZnO [24]. As shown, when the amount of CA added was 0.025 g, the absorption of ZnO in the visible range was the highest. The enhancement of optical absorption was due to the increase in the number of defect sites in the crystal

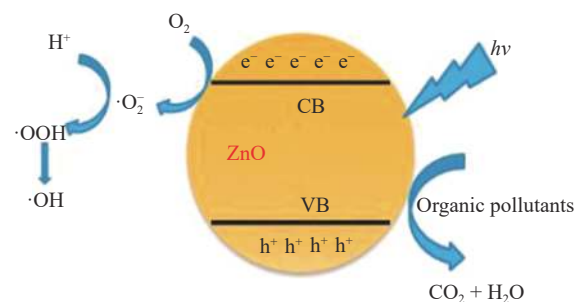
**Fig. 8. Photodegradation curves of RhB by different amounts of catalysts under (a) ultraviolet light and (b) visible light (C—Concentration of the RhB after an irradiation time (t); C₀—Concentration of the RhB after 1 h of dark treatment).**

The photocatalytic mechanism is analyzed, as shown in Fig. 9. When ZnO is irradiated by light with energy ($h\nu$) greater than its energy gap, electrons (e^-) in the valence band (VB) are excited into the CB and an equal number of holes (h^+) are left in the VB [39–40]. These photogenerated electrons (e^-) and holes (h^+) can be transferred to the surface of ZnO to participate in the redox reaction [41]. The reaction is as follows: Electrons in the CB can reduce O_2 on the surface of ZnO to superoxide anionic radicals ($\cdot O_2^-$) and further react to obtain hydroxyl radicals ($\cdot OH$) because of the strong reducibility of e^- [42–43]. At the same time, the photogenerated holes (h^+) can directly oxidize OH^- and H_2O in the aqueous solution to form $\cdot OH$. Hydroxyl radicals can decompose

structure of the catalyst, which could inhibit carrier recombination and improve the photocatalytic activity of the catalyst [35–36].

The photocatalytic performance of ZnO synthesized with different amounts of CA added was measured through the degradation of RhB under ultraviolet light and visible light irradiation. As shown in Fig. 8(a), the absorption value of RhB at the maximum absorption peak ($\lambda = 554$ nm) gradually decreased with the increase in light duration. In addition, different amounts of CA added to ZnO had different degradation rates for RhB. When the amount of CA added was 0.025 g, the degradation rate of ZnO for RhB was the highest. The degradation efficiency of ZnO for RhB with the addition of 0.025 g CA reached 99.6% when the degradation time was 1 h. Therefore, the assumption was made that RhB had been completely degraded. Fig. 8(b) shows the photodegradation curves of RhB under visible light degradation. Notably, the ZnO sample could degrade organic pollutants under visible light because of the existence of defects, consistent with that displayed in the DRS image (Fig. 7(b)) [24,37]. Simultaneously, a large specific surface area could increase the concentration of defects and improve the catalytic efficiency of visible light [29,38].

RhB molecules into carbon dioxide and water molecules [44–45].

**Fig. 9. Diagram of the photocatalytic mechanism.**

4. Conclusion

In summary, morphologically specific ZnO was synthesized through the solvothermal method using CA as an additive. After a series of tests, it was determined that the product was a hexagonal wurtzite ZnO with good crystallinity. Spherical ZnO wrapped in nanosheets was synthesized through the secondary crystallization of Zn^{2+} . Similarly, the formation of nanosheets exposed the (0001) active crystal plane of ZnO and increased the specific surface area of ZnO. Tests of the photocatalytic performance show that the degradation efficiency of ZnO for RhB was high. The photocatalytic properties of ZnO varied depending on the different amounts of CA added. The reason for this finding is that the exposure of more active crystal faces can improve the photocatalytic performance of ZnO. At the same time, the oxygen vacancy defect on the surface of ZnO can degrade RhB under visible light. Exposure of a large specific surface area can increase the concentration of defects, thus improving the photocatalytic performance.

Acknowledgements

This work was financially supported by the National Natural Science Foundation of China (No. 51602164), the Key Research Project of Shandong Province, China (No. 2017GGX40121), the Young Doctor Cooperative Fund Project (No. 2019BSHZ005), and the Scientific Research Innovation Team in Colleges and Universities of Shandong Province, China.

References

- [1] Z.Y. Jiang, X.H. Zhang, Z.M. Yuan, J.C. Chen, B.B. Huang, D.D. Dionysiou, and G.H. Yang, Enhanced photocatalytic CO_2 reduction via the synergistic effect between Ag and activated carbon in $\text{TiO}_2/\text{AC}-\text{Ag}$ ternary composite, *Chem. Eng. J.*, 348(2018), p. 592.
- [2] Z.Y. Jiang, W. Sun, W.K. Miao, Z.M. Yuan, G.H. Yang, F.G. Kong, T.J. Yan, J.C. Chen, B.B. Huang, C.H. An, and G.A. Ozin, Living atomically dispersed Cu ultrathin TiO_2 nanosheet CO_2 reduction photocatalyst, *Adv. Sci.*, 6(2019), No. 15, art. No. 1900289.
- [3] Q.L. Huang, Q.T. Zhang, S.S. Yuan, Y.C. Zhang, and M. Zhang, One-pot facile synthesis of branched Ag-ZnO heterojunction nanostructure as highly efficient photocatalytic catalyst, *Appl. Surf. Sci.*, 353(2015), p. 949.
- [4] S. Girish Kumar and K.S.R. Koteswara Rao, Tungsten-based nanomaterials (WO_3 & Bi_2WO_6): Modifications related to charge carrier transfer mechanisms and photocatalytic applications, *Appl. Surf. Sci.*, 355(2015), p. 939.
- [5] S.Q. Song, B. Cheng, N.S. Wu, A.Y. Meng, S.W. Cao, and J.G. Yu, Structure effect of graphene on the photocatalytic performance of plasmonic $\text{Ag}/\text{Ag}_2\text{CO}_3-\text{rGO}$ for photocatalytic elimination of pollutants, *Appl. Catal. B*, 181(2016), p. 71.
- [6] Y.J. Liu, H.X. Liu, H.M. Zhou, T.D. Li, and L.N. Zhang, A Z-scheme mechanism of N-ZnO/g- C_3N_4 for enhanced H_2 evolution and photocatalytic degradation, *Appl. Surf. Sci.*, 466(2019), p. 133.
- [7] S. Rehman, R. Ullah, A.M. Butt, and N.D. Gohar, Strategies of making TiO_2 and ZnO visible light active, *J. Hazard. Mater.*, 170(2009), No. 2-3, p. 560.
- [8] C.G. Tian, Q. Zhang, A.P. Wu, M.J. Jiang, Z.L. Liang, B.J. Jiang, and H.G. Fu, Cost-effective large-scale synthesis of ZnO photocatalyst with excellent performance for dye photodegradation, *Chem. Commun.*, 48(2012), No. 23, p. 2858.
- [9] E. Jang, D.W. Kim, S.H. Hong, Y.M. Park, and T.J. Park, Visible light-driven g- $\text{C}_3\text{N}_4/\text{ZnO}$ heterojunction photocatalyst synthesized via atomic layer deposition with a specially designed rotary reactor, *Appl. Surf. Sci.*, 487(2019), p. 206.
- [10] X.D. Wang, C.J. Summers, and Z.L. Wang, Large-scale hexagonal-patterned growth of aligned ZnO nanorods for nano-optoelectronics and nanosensor arrays, *Nano Lett.*, 4(2004), No. 3, p. 423.
- [11] S.T. Kochuveedu, Y.H. Jang, and D.H. Kim, A study on the mechanism for the interaction of light with noble metal-metal oxide semiconductor nanostructures for various photophysical applications, *Chem. Soc. Rev.*, 42(2013), No. 21, p. 8467.
- [12] C. Jaramillo-Páez, J.A. Navío, M.C. Hidalgo, and M. Macías, High UV- photocatalytic activity of ZnO and Ag/ZnO synthesized by a facile method, *Catal. Today*, 284(2017), p. 121.
- [13] H. Bouzid, M. Faisal, F.A. Harraz, S.A. Al-Sayari, and A.A. Ismail, Synthesis of mesoporous Ag/ZnO nanocrystals with enhanced photocatalytic activity, *Catal. Today*, 252(2015), p. 20.
- [14] R. Gupta, N.K. Eswar, J.M. Modak, and G. Madras, Ag and CuO impregnated on Fe doped ZnO for bacterial inactivation under visible light, *Catal. Today*, 300(2018), p. 71.
- [15] C. Karunakaran and P. Vinayagamoorthy, Superparamagnetic core/shell $\text{Fe}_2\text{O}_3/\text{ZnO}$ nanosheets as photocatalyst cum bactericide, *Catal. Today*, 284(2017), p. 114.
- [16] X. Zong, C.H. Sun, H. Yu, Z.G. Chen, Z. Xing, D.L. Ye, G.Q. Lu, X.Y. Li, and L.Z. Wang, Activation of photocatalytic water oxidation on N-doped ZnO bundle-like nanoparticles under visible light, *J. Phys. Chem. C*, 117(2013), No. 10, p. 4937.
- [17] K. Mahmood, H.W. Kang, S.B. Park, and H.J. Sung, Hydrothermally grown upright-standing nanoporous nanosheets of iodine-doped ZnO (ZnO:I) nanocrystallites for a high-efficiency dye-sensitized solar cell, *ACS Appl. Mater. Interfaces*, 5(2013), No. 8, p. 3075.
- [18] H.G. Yang, C.H. Sun, S.Z. Qiao, J. Zou, G. Liu, S.C. Smith, H.M. Cheng, and G.Q. Lu, Anatase TiO_2 single crystals with a large percentage of reactive facets, *Nature*, 453(2008), p. 638.
- [19] K.B. Zhou, X. Wang, X.M. Sun, Q. Peng, and Y.D. Li, Enhanced catalytic activity of ceria nanorods from well-defined reactive crystal planes, *J. Catal.*, 229(2005), No. 1, p. 206.
- [20] E.S. Jang, J.-H. Won, S.-J. Hwang, and J.-H. Choy, Fine tuning of the face orientation of ZnO crystals to optimize their photocatalytic activity, *Adv. Mater.*, 18(2006), No. 24, p. 3309.
- [21] A. McLaren, T. Valdes-Solis, G.Q. Li, and S.C. Tsang, Shape and size effects of ZnO nanocrystals on photocatalytic activity, *J. Am. Chem. Soc.*, 131(2009), No. 35, p. 12540.
- [22] Y.J. Liu, H.X. Liu, B.B. Huang, T.D. Li, and J.G. Wang, Nano needle decorated ZnO hollow spheres with exposed (0001) planes and their corrosion using acetic acid, *CrystEngComm*, 19(2017), No. 38, p. 5774.
- [23] S. He, S.T. Zhang, J. Lu, Y.F. Zhao, J. Ma, M. Wei, D.G. Evans, and X. Duan, Enhancement of visible light photocatalysis by grafting ZnO nanoplatelets with exposed (0001) facets onto a hierarchical substrate, *Chem. Commun.*, 47(2011), No.

- 38, p. 10797.
- [24] J.P. Wang, Z.Y. Wang, B.B. Huang, Y.D. Ma, Y.Y. Liu, X.Y. Qin, X.Y. Zhang, and Y. Dai, Oxygen vacancy induced band-gap narrowing and enhanced visible light photocatalytic activity of ZnO, *ACS Appl. Mater. Interfaces*, 4(2012), No. 8, p. 4024.
- [25] E. Grabowska, J.W. Sobczak, M. Gazda, and A. Zaleska, Surface properties and visible light activity of W-TiO₂ photocatalysts prepared by surface impregnation and sol-gel method, *Appl. Catal. B*, 117-118(2012), p. 351.
- [26] X.B. Chen, L. Liu, P.Y. Yu, and S.S. Mao, Increasing solar absorption for photocatalysis with black hydrogenated titanium dioxide nanocrystals, *Science*, 331(2011), No. 6018, p. 746.
- [27] X.J. Bai, L. Wang, R.L. Zong, Y.H. Lv, Y.Q. Sun, and Y.F. Zhu, Performance enhancement of ZnO photocatalyst via synergistic effect of surface oxygen defect and graphene hybridization, *Langmuir*, 29(2013), No. 9, p. 3097.
- [28] J.C. Wang, P. Liu, X.Z. Fu, Z.H. Li, W. Han, and X.X. Wang, Relationship between oxygen defects and the photocatalytic property of ZnO nanocrystals in nafion membranes, *Langmuir*, 25(2009), No. 2, p. 1218.
- [29] J. Wang, Y. Xia, Y. Dong, R.S. Chen, L. Xiang, and S. Komarneni, Defect-rich ZnO nanosheets of high surface area as an efficient visible-light photocatalyst, *Appl. Catal. B*, 192(2016), p. 8.
- [30] H.F. Greer, W.Z. Zhou, G. Zhang, and H. Ménard, Nanocone decorated ZnO microspheres exposing the (0001) plane and enhanced photocatalytic properties, *Adv. Mater. Interfaces*, 4(2017), No. 13, art. No. 1601238.
- [31] V.K. LaMer and R.H. Dinegar, Theory, production and mechanism of formation of monodispersed hydrosols, *J. Am. Chem. Soc.*, 72(1950), No. 11, p. 4847.
- [32] H. Reiss, The growth of uniform colloidal dispersions, *J. Chem. Phys.*, 19(1951), No. 4, p. 482.
- [33] S.G. Kwon and T. Hyeon, Formation mechanisms of uniform nanocrystals via hot-injection and heat-up methods, *Small*, 7(2011), No. 19, p. 2685.
- [34] H. Wang, C.C. Wang, Q.F. Chen, B.S. Ren, R.F. Guan, X.F. Cao, X.P. Yang, and R. Duan, Interface-defect-mediated photocatalysis of mesocrystalline ZnO assembly synthesized *in-situ* via a template-free hydrothermal approach, *Appl. Surf. Sci.*, 412(2017), p. 517.
- [35] O. Bechambi, M. Chalbi, W. Najjar, and S. Sayadi, Photocatalytic activity of ZnO doped with Ag on the degradation of endocrine disrupting under UV irradiation and the investigation of its antibacterial activity, *Appl. Surf. Sci.*, 347(2015), p. 414.
- [36] Y. Haldorai, A. Rengaraj, C.H. Kwak, Y.S. Huh, and Y.-K. Han, Fabrication of nano TiO₂@graphene composite: Reusable photocatalyst for hydrogen production, degradation of organic and inorganic pollutants, *Synth. Met.*, 198(2014), p. 10.
- [37] X.X. Wei, H.T. Cui, S.Q. Guo, L.F. Zhao, and W. Li, Hybrid BiOBr-TiO₂ nanocomposites with high visible light photocatalytic activity for water treatment, *J. Hazard. Mater.*, 263(2013), p. 650.
- [38] R. Ghosh Chaudhuri and S. Paria, Visible light induced photocatalytic activity of sulfur doped hollow TiO₂ nanoparticles, synthesized via a novel route, *Dalton Trans.*, 43(2014), No. 14, p. 5526.
- [39] L.O. de B. Benetoli, B.M. Cadorin, C. da S. Postiglione, I.G. de Souza, and N.A. Debacher, Effect of temperature on methylene blue decolorization in aqueous medium in electrical discharge plasma reactor, *J. Braz. Chem. Soc.*, 22(2011), No. 9, p. 1669.
- [40] C.-H. Wu and J.-M. Chern, Kinetics of photocatalytic decomposition of methylene blue, *Ind. Eng. Chem. Res.*, 45(2006), No. 19, p. 6450.
- [41] H. Esmaili, A. Kotobi, S. Sheibani, and F. Rashchi, Photocatalytic degradation of methylene blue by nanostructured Fe/FeS powder under visible light, *Int. J. Miner. Metall. Mater.*, 25(2018), No. 2, p. 244.
- [42] S. Gao, W.Y. Yang, J. Xiao, B. Li, and Q. Li, Creation of passivated Nb/N p-n co-doped ZnO nanoparticles and their enhanced photocatalytic performance under visible light illumination, *J. Mater. Sci. Technol.*, 35(2019), No. 4, p. 610.
- [43] X.W. Zhang, X.L. Zhang, X. Wang, L.Q. Liu, J.H. Ye, and D.F. Wang, Enhancing the photocatalytic activity and photostability of zinc oxide nanorod arrays via graphitic carbon mediation, *Chin. J. Catal.*, 39(2018), No. 5, p. 973.
- [44] W.L. Yu, J.F. Zhang, and T.Y. Peng, New insight into the enhanced photocatalytic activity of N-, C- and S-doped ZnO photocatalysts, *Appl. Catal. B*, 181(2016), p. 220.
- [45] R.Q. Gao, Q. Sun, Z. Fang, G.T. Li, M.Z. Jia, and X.M. Hou, Preparation of nano-TiO₂/diatomite-based porous ceramics and their photocatalytic kinetics for formaldehyde degradation, *Int. J. Miner. Metall. Mater.*, 25(2018), No. 1, p. 73.